Twente Optical Perfusion Camera: system overview and performance for video rate laser Doppler perfusion imaging

Matthijs Draijer, Erwin Hondebrink, Ton van Leeuwen[*] and Wiendelt Steenbergen

Biophysical Engineering Group, Institute for Biomedical Technology, University of Twente, Enschede, The Netherlands
[*] Also Biomedical Engineering & Physics, Academic Medical Center, University of Amsterdam, Amsterdam, the Netherlands

w.steenbergen@utwente.nl

Abstract: We present the Twente Optical Perfusion Camera (TOPCam), a novel laser Doppler Perfusion Imager based on CMOS technology. The tissue under investigation is illuminated and the resulting dynamic speckle pattern is recorded with a high speed CMOS camera. Based on an overall analysis of the signal-to-noise ratio of CMOS cameras, we have selected the camera which best fits our requirements. We applied a pixel-by-pixel noise correction to minimize the influence of noise in the perfusion images. We can achieve a frame rate of 0.2 fps for a perfusion image of 128×128 pixels (imaged tissue area of 7×7 cm^2) if the data is analyzed online. If the analysis of the data is performed offline, we can achieve a frame rate of 26 fps for a duration of 3.9 seconds. By reducing the imaging size to 128×16 pixels, this frame rate can be achieved for up to half a minute. We show the fast imaging capabilities of the system in order of increasing perfusion frame rate. First the increase of skin perfusion after application of capsicum cream, and the perfusion during an occlusion-reperfusion procedure at the fastest frame rate allowed with online analysis is shown. With the highest frame rate allowed with offline analysis, the skin perfusion revealing the heart beat and the perfusion during an occlusion-reperfusion procedure is presented. Hence we have achieved video rate laser Doppler perfusion imaging.

© 2009 Optical Society of America

OCIS codes: (170.3340) Laser Doppler velocimetry; (170.3890) Medical optics instrumentation; (170.4580) Optical diagnostics for medicine; (170.1650) Coherence imaging

---

References and links

1. R. Bonner and R. Nossal, "Model for Laser Doppler Measurements of Blood Flow in Tissue," Appl. Opt. **20**, 2097–2107 (1981).
2. Y. Aizu and T. Asakura, "Bio-Speckle Phenomena and Their Application to The Evaluation Of Blood Flow," Opt. Laser Technol. **23**, 205–219 (1991).
3. A. Serov, W. Steenbergen, and F. F. M. de Mul, "Laser Doppler Perfusion Imaging With A Complimentary Metal Oxide Semiconductor Image Sensor," Opt. Lett. **27**, 300–302 (2002).
4. J. D. Briers, "Laser Doppler and Time-Varying Speckle: A reconciliation," J. Opt. Soc. Am. A **13**, 45–350 (1996).

5. J. D. Briers, "Laser Doppler, Speckle and Related Techniques for Blood Perfusion Mapping and Imaging," Physiological Measurements **22**, R35–R66 (2001).
6. C. J. Stewart, R. Frank, K. R. Forrester, J. Tulip, R. Lindsay, and R. C. Bray, "A comparison of two laser-based methods for determination of burn scar perfusion: Laser Doppler versus laser speckle imaging," Burns **31**, 744–752 (2005).
7. M. J. Draijer, E. Hondebrink, T. G. van Leeuwen, and W. Steenbergen, "Connecting laser Doppler perfusion imaging and laser speckle contrast analysis," in *Optical Diagnostics and Sensing VIII*, G. L. Coté and A. V. Priezzhev, eds., vol. 6863 of *Proc. SPIE*, pp. 68,630C–68,630C–8 (2008).
8. A. F. Fercher and J. D. Briers, "Flow Visualization By Means of Single-Exposure Speckle Photography," Opt. Commun. **37**, 326–330 (1981).
9. J. D. Briers, G. Richards, and X. W. He, "Capillary Blood Flow Monitoring Using Laser Speckle Contrast Analysis (LASCA)," J. Biomed. Opt. **4**, 164–175 (1999).
10. M. Draijer, E. Hondebrink, T. van Leeuwen, and W. Steenbergen, "Review of laser speckle contrast techniques for visualizing tissue perfusion," Lasers Med. Sci. (2008).
11. H. Cheng, Q. Luo, S. Zeng, S. Chen, J. Cen, and H. Gong, "Modified laser speckle imaging method with improved spatial resolution," J. Biomed. Opt. **8**, 559–564 (2003).
12. H. Cheng and T. Q. Duong, "Simplified laser-speckle-imaging analysis method and its application to retinal blood flow imaging," Opt. Lett. **32**, 2188–2190 (2007).
13. Z. B. M. Niazi, T. J. H. Essex, R. Rapini, D. Scott, N. R. McLean, and M. J. M. Black, "New Laser Doppler Scanner, A Valuable Adjunct in Burn Depth Assessment," Burns **19**, 485–489 (1993).
14. S. A. Pape, C. A. Skouras, and P. O. Byrne, "An audit of the use of laser Doppler imaging (LDI) in the assessment of burns of intermediate depth," Burns **27**, 233–239(7) (2001).
15. F. W. Kloppenberg, G. I. Beerthuizen, and H. J. ten Duis, "Perfusion of burn wounds assessed by laser Doppler imaging is related to burn depth and healing time," Burns **27**, 359–363 (2001).
16. E. J. Droog, W. Steenbergen, and F. Sjoberg, "Measurement of Depth of Burns By Laser Doppler Perfusion Imaging," Burns **27**, 561–568 (2001).
17. R. Bray, K. Forrester, C. Leonard, R. McArthur, J. Tulip, and R. Lindsay, "Laser Doppler Imaging of Burn Scars: A Comparison of Wavelength And Scanning Methods," Burns **29**, 199–206 (2003).
18. E. La Hei, A. Holland, and H. Martin, "Laser Doppler Imaging of paediatric burns: Burn wound outcome can be predicted independent of clinical examination," Burns **32**, 550–553 (2006).
19. A. K. Dunn, H. Bolay, M. A. Moskowitz, and D. A. Boas, "Dynamic Imaging of Cerebral Blood Flow Using Laser Speckle," J. Cereb. Blood Flow Metab. **21**, 195–201 (2001).
20. F. F. M. de Mul, J. Blaauw, J. G. Aarnoudse, A. J. Smit, and G. Rakhorst, "Diffusion model for iontophoresis measured by laser-Doppler perfusion flowmetry, applied to normal and preeclamptic pregnancies," J. Biomed. Opt. **12**, 14,032 – 1 (2007).
21. A. Serov, B. Steinacher, and T. Lasser, "Full-Field Laser Doppler Perfusion Imaging and Monitoring With An Intelligent CMOS Camera," Opt. Express **13**, 3681–3689 (2005).
22. A. Serov and T. Lasser, "High-speed laser Doppler perfusion imaging using an integrating CMOS image sensor," Opt. Express **13**, 6416–6428 (2005).
23. M. J. Draijer, E. Hondebrink, W. Steenbergen, and T. G. van Leeuwen, "Laser Doppler Perfusion Imaging with a high-speed CMOS-camera," in *Novel Optical Instrumentation for Biomedical Applications III*, C. D. Depeursinge, ed., vol. 6631 of *Proc. SPIE*, p. 66310N (2007).
24. A. Serov, W. Steenbergen, and F. de Mul, "Prediction of the photodetector signal generated by Doppler-induced speckle fluctuations: theory and some validations," J. Opt. Soc. Am. A **18**, 622–630 (2001).
25. E. Hecht, *Optics*, 3rd ed. (Addison-Wesley, 1998).
26. G. Rieke, *Detection of Light*, 2nd ed. (Cambridge University Press, 2003).
27. A. Humeau, J. L. Saumet, and J. P. L. Huillier, "Simplified Model of Laser Doppler Signals During Reactive Hyperaemia," Medical & Biological Engineering & Computing **38**, 80–87 (2000).
28. Q. Gu, B. R. Hayes-Gill, and S. P. Morgan, "Laser Doppler blood flow complementary metal oxide semiconductor imaging sensor with analog on-chip processing," Appl. Opt. **47**, 2061–2069 (2008).

1. Introduction

Laser Doppler Perfusion Imaging (LDPI) [1–7] and related techniques like Laser Speckle Contrast Analysis (LASCA) [4–6, 8–10] and Laser Speckle Imaging (LSI) [11, 12] are established techniques for determining skin perfusion maps, for instance to diagnose burns [6, 13–18], to study cerebral blood flow in small animals [19], and for drug uptake studies (e.g., using iontophoresis) [20].

In commercially available LDPI devices the area under investigation is scanned with a narrow laser beam. Using beam scanning, obtaining a perfusion image of 64×64 pixels takes
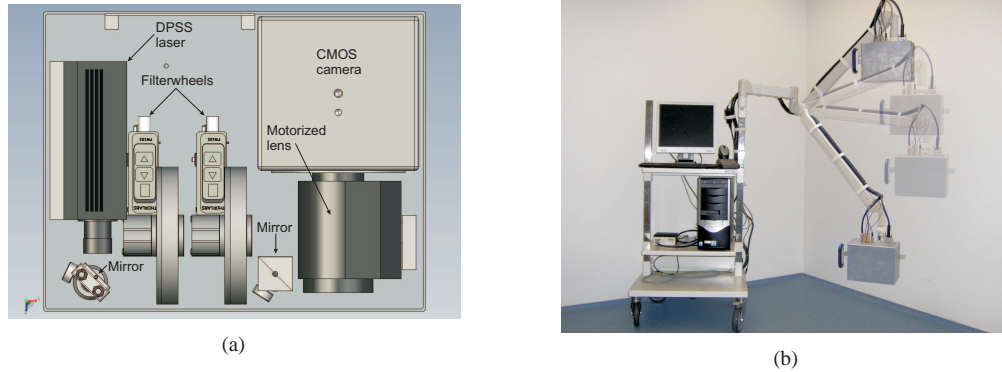
Fig. 1: (a) Schematic overview of the measurement head (footprint $21,5 \times 28$ cm) and (b) photo of the entire TOPCam system.

approximately 3 minutes. This long scanning time impedes the observation of fast perfusion changes, for instance during reperfusion after occlusion. To obtain real time reperfusion images a refresh rate of approximately 25 Hz is needed. Also from the perspective of the patient it is sometimes strongly desirable to have a short imaging time, e.g., for burn patients, and in general for young children and elder patients.

Here we present the Twente Optical Perfusion Camera (TOPCam), a novel laser Doppler Perfusion Imager based on CMOS technology [3, 21–23] which allows real time acquisition of dynamic laser speckle patterns generated by the tissue perfusion. We discuss various instrumental aspects and present performance studies on phantoms and *in-vivo* measurements.

2. The Twente Optical Perfusion Camera

A schematic overview and a photo of the TOPCam is shown in Fig. 1. The TOPCam is equipped with a 671 nm DPSS laser with a power of 400 mW (ML-III-671, CNI-laser). By a mirror the laser light is guided through two filter wheels, which contain filters for adjusting the light intensity by use of a neutral density filter and the beam shape by an engineered diffuser (RPC Photonics). This engineered diffuser transforms the laser beam to a homogeneous square (5% spatial variation in homogenity) of approximately 7×7 centimeter at 40 cm distance (i.e., the normal working distance). With another mirror the laser light is directed toward the skin. Backscattered laser light from the skin is focused with a motorized zoom lens (lens : T6Z5710M-CS, Computar; controler : CBZ230, Computar) on the high speed CMOS camera (Fastcam 1024PCI, Photron) which can achieve a frame rate of 27 kHz for an area of 128×128 pixels. Using that frame rate, 1024 raw speckle images were recorded and transfered to the computer for analysis. The time trace for every pixel was Fourier transformed using FFT and the power spectrum $S(\omega)$ is obtained. Perfusion maps are generated by calculating for each pixel the first moment of the power spectrum according to :

$$M_1 = \int_{50Hz}^{13.5kHz} \omega S(\omega)d\omega \tag{1}$$

To normalize the perfusion image for the amount of light reflected from the tissue, the perfusion image was divided by the DC image (i.e., the mean pixel-by-pixel intensity values), as is commonly used in commercially available laser Doppler perfusion imagers.
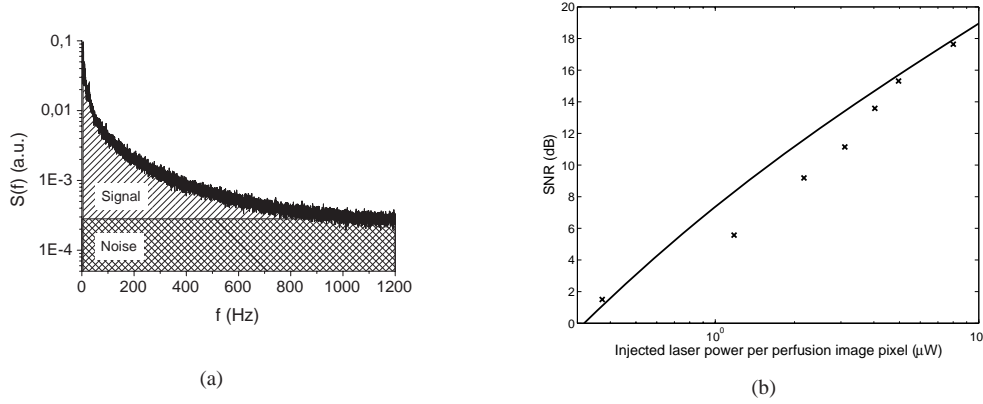
Fig. 2: (a) schematic overview of the signal part (/-hatched) and noise part (×-hatched) for determining the SNR from the power spectrum. (b) comparison between the measured SNR (×) and the SNR (solid line) calculated with Eq. (2).

2.1. Camera selection based on signal-to-noise ratio

To select the high speed camera which fits our requirements the best, we predicted the signal-to-noise ratio (SNR) of several cameras, based on their specifications.

In LDPI the signal is formed by the AC-component of the time fluctuating photo current (i_{AC}). So the SNR is defined as :

$$SNR_{CMOS} = \frac{\langle i_{AC}^2 \rangle}{\langle i_{noise}^2 \rangle} \tag{2a}$$

The AC-component of the laser Doppler signal can be written as [24]:

$$\langle i_{AC}^2 \rangle = \gamma(2-\gamma)\frac{\langle i_{DC} \rangle^2}{2N} \tag{2b}$$

with γ the fraction Doppler-shifted photons, N the number of speckles per pixel and i_{DC} the DC-component of the photo current. Furthermore we have assumed the backscattered light to be completely depolarised, leading to a factor 2 in the denominator of Eq. (2b). Under the assumption of a homogeneous laser beam, homogeneous and isotropic diffuse backscattering, this DC-component is given by [25] :

$$\langle i_{DC} \rangle = \frac{k_{back}P_{laser}}{\#_{pixels}}\frac{\pi r^2}{4\pi Z^2}\frac{\lambda}{hc}\eta Q q_e \tag{2c}$$

with k_{back} the diffuse reflectivity of the tissue, P_{laser} the laser power, $\#_{pixels}$ the number of pixels over which the laser light is divided, r the radius of the lens, Z the distance between the lens and the sample, λ the laser wavelength, h the constant of Planck, c the speed of light, η the fill factor of the CMOS chip, Q the quantum efficiency of the CMOS chip and q_e the charge of one electron.

The number of speckles on one pixel (N) is equal to the ratio of the area of the pixel (A_{pixel}) to the speckle area ($A_{speckle}$) :

$$N = \frac{A_{pixel}}{A_{speckle}} \tag{2d}$$

Table 1: Values of the different parameters in Eq. (2) used to predict the SNR of several high speed CMOS cameras.

parameter	CCi4	Redlake HS-4	Phantom V7.1	1024PCI FastCam
λ (nm)	632	671	671	671
r (mm)	17	14	14	14
γ	1	0.1	0.1	0.1
k_{back} [a]	0.5	0.5	0.5	0.5
f_{sample} (kHz)	3.3	30	30	30
B_R (kHz)	20	100	100	100
image size (px)	40×40	128×128	128×128	128×128
imaged area (cm)	$\varnothing 2$	5×5	5×5	5×5
R (mm)	17.526 [b]	17.526 [b]	17.526 [b]	17.526 [b]
Z (cm)	85	42.8	31.1	40.3
pixel pitch (μm)	7	16	22	17
Q	0.2	0.37	0.4	0.3
fill factor	0.6	0.62	0.65	0.6
bit depth	10	8	10	10
well capacity (electrons)	55e3	60e3	80e3	60e3

[a] based on Monte Carlo simulations.

[b] defined distance for a C-mount lens.

The speckle size is given by :

$$A_{speckle} = \frac{\lambda^2}{\Omega} = \lambda^2 \frac{R^2}{\pi r^2} \qquad (2e)$$

with Ω the solid angle of the lens on the CMOS chip and R the distance between the lens and the CMOS chip. The noise is composed of shot noise ($2q_e \langle i_{DC} \rangle$), dark noise ($2q_e i_{dark}$) and quantization noise ($2q_e i_{AD}$) (i.e., i_{AD} is the current which corresponds to the number of quantization electrons, which equals the well capacity divided by the number of bit levels) [26] :

$$\langle i_{noise}^2 \rangle = 2q_e \left(\langle i_{DC} \rangle + i_{dark} + i_{AD} \right) B_R \qquad (2f)$$

with B_R the bandwidth of the high speed CMOS camera.

To test how accurately the SNR can be predicted by Eq. (2a)-(2f), we measured and calculated the SNR for a CMOS camera available in our lab (CCi4, C-Cam). The parameters which are used to calculate the SNR according to Eq. (2) are shown in table 1. To measure the SNR we obtained the perfusion map of a Delrin disk with a hole filled with *IntraLipid 4%* (Fresenius Kabi) for different light intensities (i.e., different P_{laser} in Eq. (2c)). As laser source we used a 10 mW HeNe laser with a wavelength of 632 nm. With a lens the laser beam was enlarged to a diameter of approximatly 2 cm. To vary the amount of light falling on the sample a rotatable polarizer was positioned between the laser and the sample. Based on the laser Doppler signal from the area with *IntraLipid*, we determined the power spectrum. From this power spectrum we extracted the SNR : the average amplitude of the plateau for higher frequencies was taken to be the noise level. The noise part was determined by calculating the area under the noise level. The signal part was taken by calculating the area under the power spectrum after subtracting the noise part. This is schematicaly shown in Fig. 2(a). The SNR was determined by dividing the
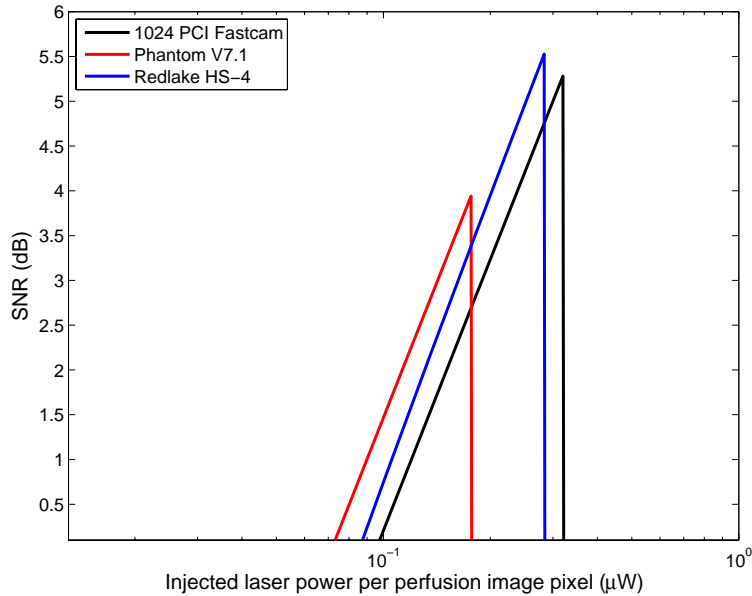
Fig. 3: The predicted SNR for possible CMOS cameras in high speed LDPI as a function of injected laser power per perfusion image pixel.

signal part by the noise part. Figure 2(b) shows a comparison between the average measured SNR in 10×10 pixels and the calculated SNR based on Eq. (2).

Figure 2(b) shows that the predictions provided by Eq. (2a)-(2f) are sufficiently accurate to be used as a tool for selection of a CMOS camera for LDPI. Figure 3 shows the predicted SNR for several high speed cameras which we considered for LDPI. The parameters which are used to calculate the SNR are shown in table 1. The well capacity is the number of electrons a pixel can detect before getting saturated. This number is used to determine the amount of injected laser power which saturates the camera and results in a SNR of 0. In the simulations the image size is kept constant at 128×128 pixels while the imaged tissue area is taken equal to 5×5 cm^2, resulting in a constant laser power per pixel (i.e., constant i_{DC}) and a different magnification for all cameras. As expected, more laser power will increase the SNR. The main reason for the higher SNR for the Phantom compared to the Redlake and FastCam is the difference in quantum efficiency Q in Eq. (2c). The truncation of the predicted SNR values for a certain laser power is due to saturation of the pixels. With a certain amount of light falling on a pixel, the well is completely filled and $\langle i_{AC} \rangle$ drops to 0 resulting in a SNR of 0. The highest SNR for a given amount of injected light can be obtained by the *Redlake HS-4*, however, in practical use we found both cameras to be equivalent so we have selected the *1024PCI FastCam*.

2.2. *Noise correction*

Noise in the generated raw signals will lead to an offset in the measured perfusion values. To correct for that, we measured for all pixels individually the perfusion signal as a function of the amount of light backscattered from a block of Delrin, illuminated by light of a light emitting diode (LED) of 630 nm. The light from a LED is incoherent and Delrin is a static medium, so all perfusion signal can be classified as noise. A 3rd order fit through these measurements results in a noise correction curve for each pixel. Examples of measured noise curves (i.e., M_1 as a function of the DC value) for 2 separate pixels, measured on 2 separate days, and the 3rd
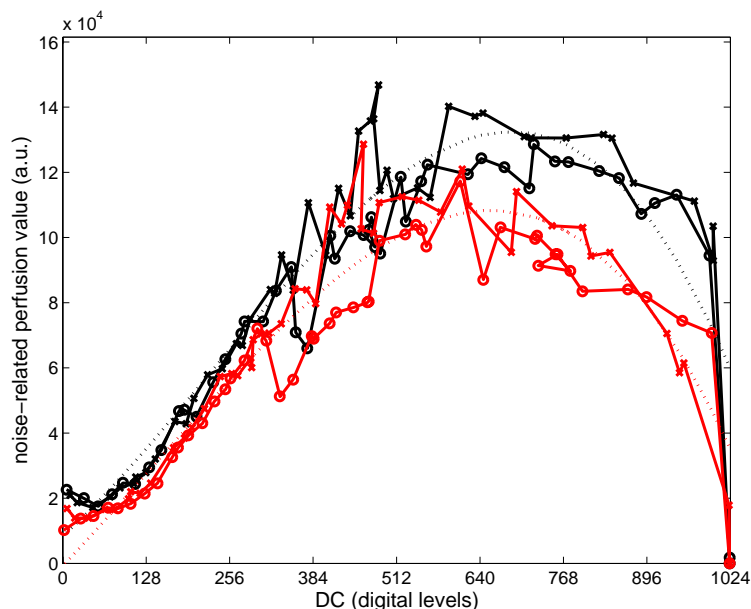
Fig. 4: Typical examples of the perfusion values due to noise as a function of DC on day 1 (o), day 4 (x) and the correction curves based on a 3rd order fit (dashed lines).

order fits (i.e., best fit through the data of both days) are shown in Fig. 4. An increase in DC results in an increase in shot noise in Eq. 2f, which explains the larger noise with increasing DC. The exact reason for the decrease after 650 digital levels is not known yet. In view of our experience with other cameras, we believe that this is a feature of the specific device. The end result of noise-estimation based on the asymptotic value of the power spectrum, or based on the detected DC level will be the same. However, during measurements the use of the DC level for noise estimation algorithmically more simple.

Based on the DC-value of each pixel, the measured perfusion value can be corrected by subtraction of a value given by the 3rd order correction function. Figure 5 shows a DC-normalized uncorrected as well as noise-corrected perfusion image for a circular piece of Delrin with holes of various diameter, placed on green surgery paper. The hole of 4 mm in diameter was filled with *IntraLipid 20%*.

2.3. Speed performance of system

Table 2 gives an overview of the current speed of the TOPCam in numbers for two different image sizes (i.e., 128×128 pixels and 128×16 pixels). The TOPCam can be used in two different modes of data analysis, referred to as online and offline. In the online mode the data for a single perfusion frame are recorded and immediately analyzed before the next measurement is performed. In the offline mode the analysis is postponed, first the data for all measurements are recorded and afterwards the data are analyzed. The online mode allows for a measurement series of unlimited duration, with the perfusion frame rate limited by the transfer speed of the camera (0.2 fps). In the offline mode, a maximum perfusion framerate of 26 fps can be achieved that is related to the raw image capture frame rate. The duration of a recording in offline mode is limited by the memory of the camera, as indicated in table 2. The table also indicates that the reduction in time is not linear with the amount of data transferred or the amount of data stored. This is probably caused by overhead in the data-transfer and storage (e.g., handshaking in the
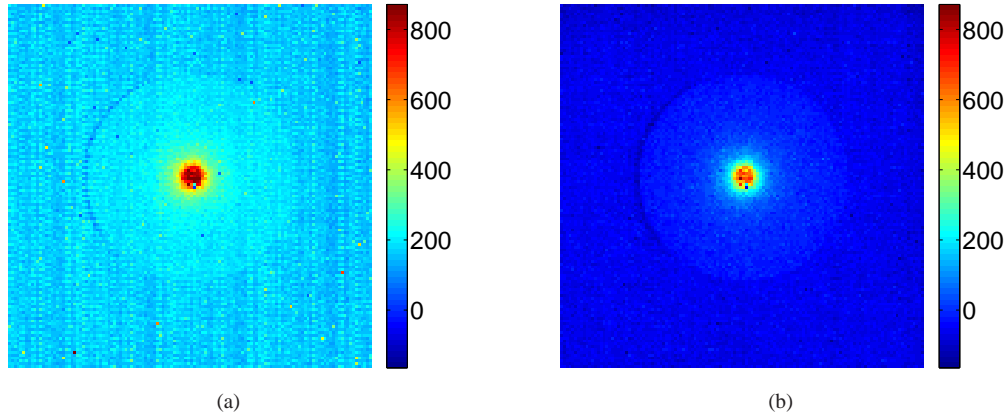
Fig. 5: (a) DC-normalized raw perfusion image (128×128 pixels) of a piece of Delrin of 40 mm in diameter with a hole of 4 mm in diameter, placed on green surgery paper. The hole was filled with *IntraLipid 20%*. (b) the DC-normalized noise corrected perfusion image of the same sample.

transfer-protocol, time needed by the computer to creating a file -regardless of the image size-).

3. Demonstration of real time imaging capabilities

The main advantage of the TOPCam over commercially available LDPI devices is the imaging speed. In this section examples of the faster imaging opportunities of the TOPCam will be shown.

Table 2: Overview of the system speed averaged over 5 measurements for an 10-bits recording of a sequence of 1024 raw images at a frame rate of 27 kHz.

	128×128 px	128×16 px
data acquisition (msec)	38	38
data transfer (msec)	3096	2705
storage (msec)	1366	1150
signal processing (msec)	998	159
length of offline perfusion recording with current memory[a](sec)	3.87	30.95
length of offline perfusion recording with with maximal memory[b] (sec)	46.44 [c]	371.40 [c]

[a] current memory is 2 Gb

[b] maximal memory is 24 Gb

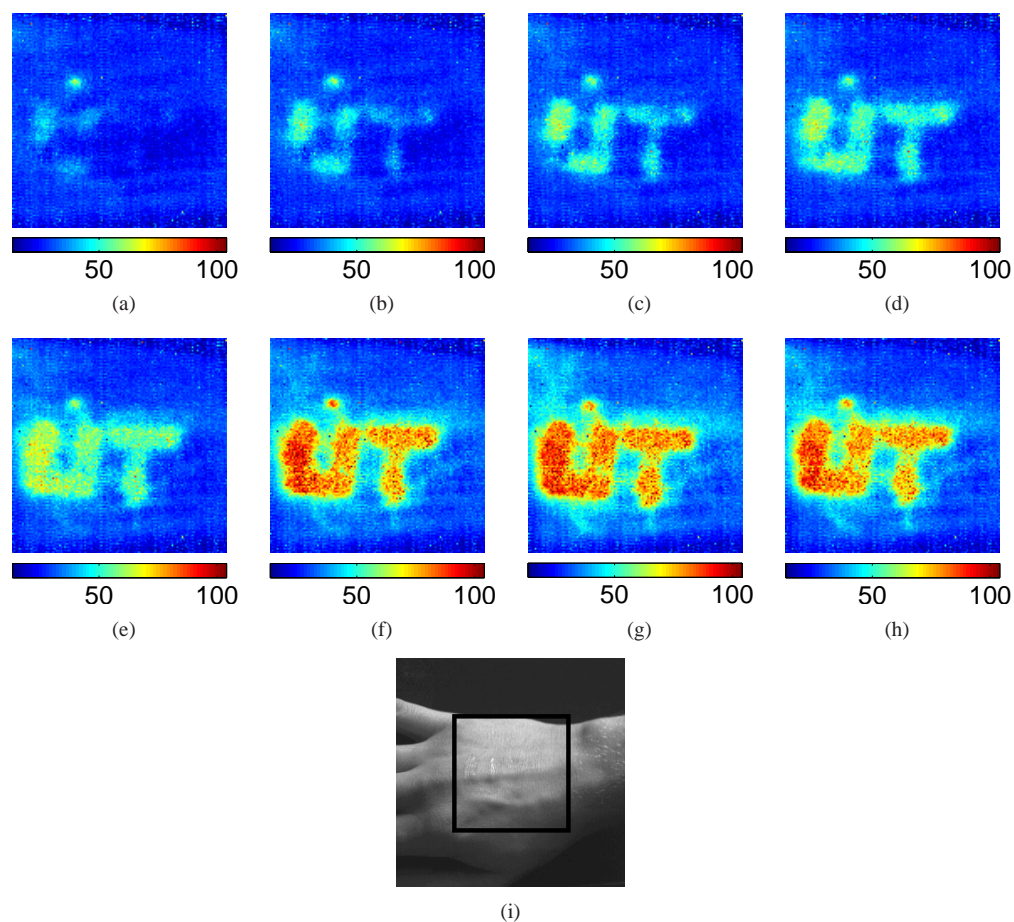[c] based on extrapolation of current amount of memory

Fig. 6: The letters UT ('University of Twente') written with capsicum cream on the back of the hand of a volunteer. DC-normalized perfusion image (128 × 128 pixels) after (a) 3:41 min, (b) 4:32 min, (c) 5:13 min, (d) 7:14 min, (e) 11:36 min, (f) 12:08 min, (g) 13:48 min and (h) 15:13 min (Media 1). (i) Photo of the hand taken with the CMOS camera, the black square indicates the area in which the perfusion is measured.
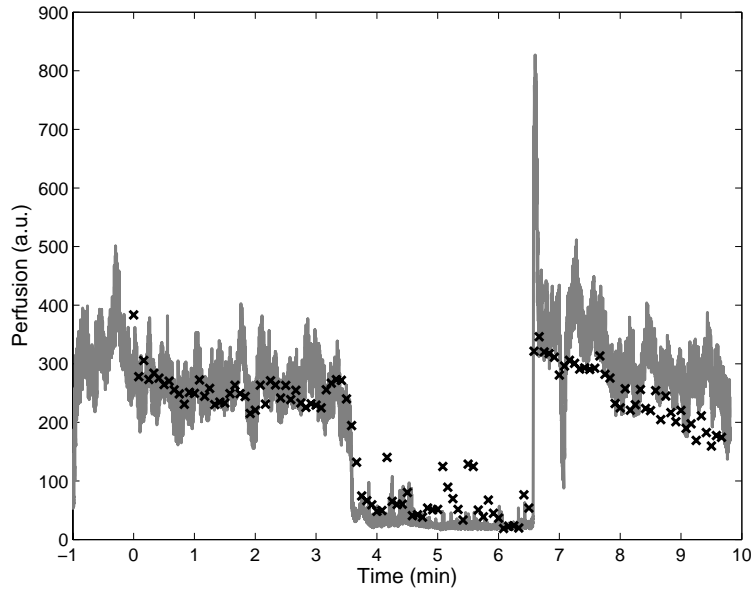
Fig. 7: Comparison of the readings of the TopCAM (x) and the Periflux5000 (Perimed, Sweden) during an occlusion-reperfusion procedure on the wrist of a volunteer (Media 2).

3.1. Methods and results

3.1.1. Online recording

For the first example the online mode was chosen to follow an increase in perfusion over a longer period of time (e.g 15 minutes). With capsicum cream (Midalgan, Remark Groep BV, Meppel, the Netherlands), a perfusion increasing cream, the letters UT were written on the dorsal side of the hand of the subject (male, 32 yr). Immediately after application of the cream the measurement was started and approximately every 45 seconds a perfusion measurement was performed. Figure 6 shows a selection of the sequence of DC-normalized perfusion images as well as a photo taken with the CMOS camera, the black square indicates the area in which is measured. Normal perfusion is indicated by blue whereas increased perfusion is shown in red. The images show a clear increase in perfusion over time due to the cream.

To investigate how the reading of the TOPCam corresponds to the reading of a commercially available fiber optic laser Doppler flow meter, we used the TOPCam in online mode together with the Periflux5000 with fiberoptic probe 145-198 (Permed AB, Sweden). Measurements were performed on the thenar eminence (Periflux5000) and the wrist (TopCam) of a healthy subject (male, 26 yr). The Periflux5000 recorded 32 samples per second whereas the TOPCam recorded a perfusion image every 5 seconds. The Periflux5000 and TOPCam can not measure at the same location so the probe of the Periflux5000 was placed next to the area imaged by the TOPCam. Approximately 3.5 minutes after starting the TOPCam measurement occlusion was applied by inflating a blood pressure cuff around the upper arm of the subject. After 3 minutes the occlusion was released and the measurements continued for another 3 minutes [27]. Figure 7 shows the result of this comparison. The value for the perfusion of the TOPCam is obtained by taking the average value of the whole perfusion image after noise correction and normalization with DC. The reading of the Periflux5000 is multiplied with a factor 3.6 to scale it with the TOPCam. A clear decrease during the occlusion and an increase after the occlusion are present.
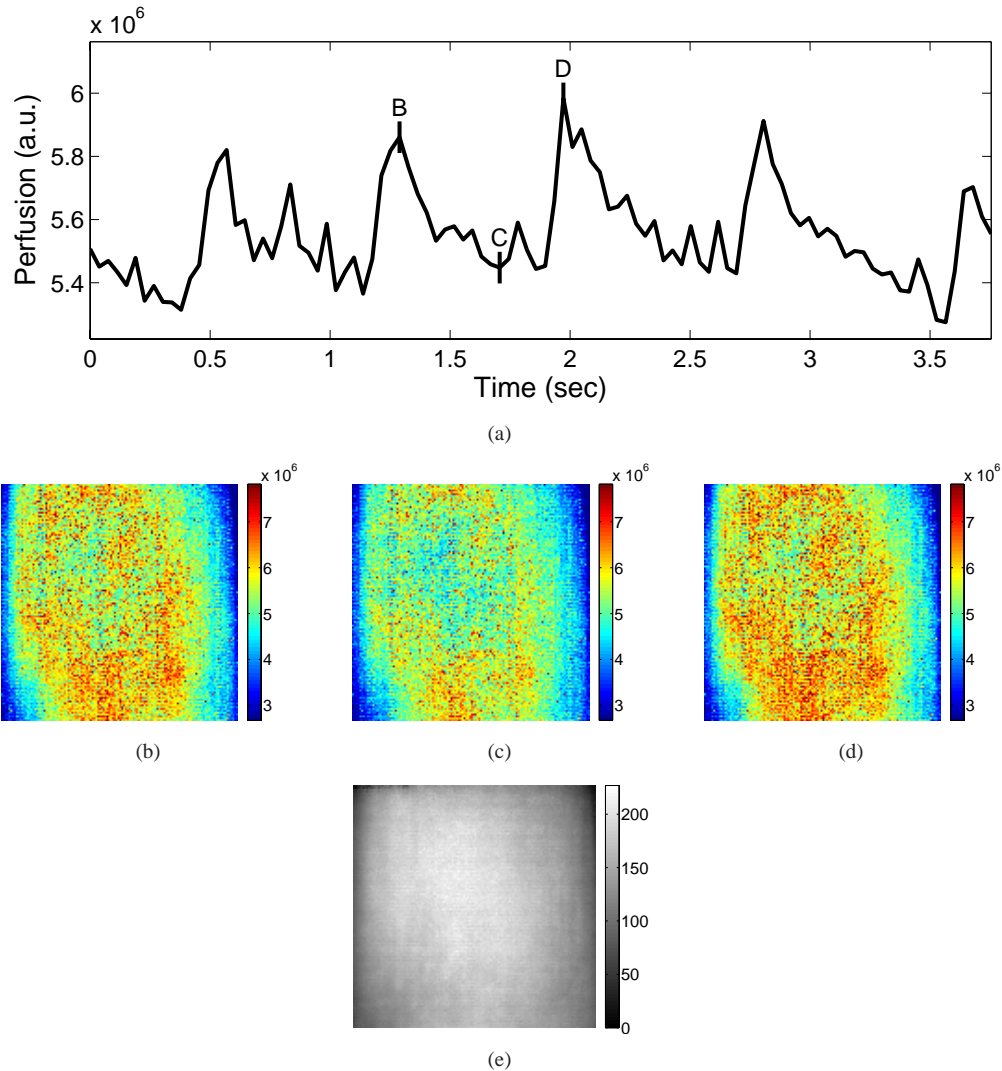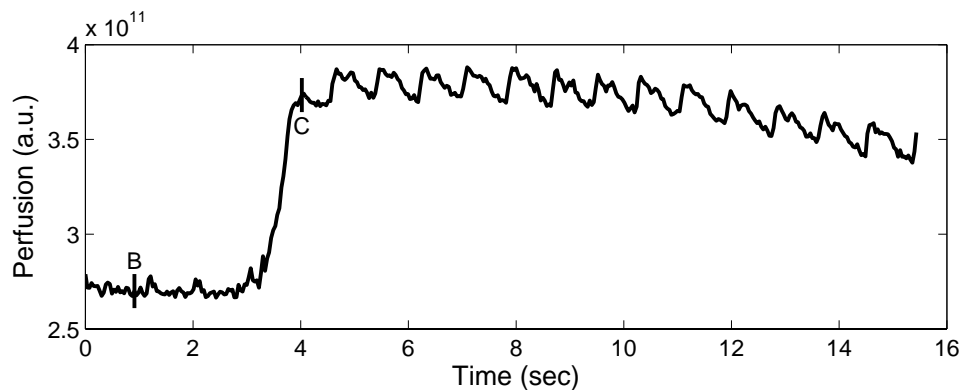
Fig. 8: Continuous recording of 128×128 pixel perfusion images in the hand of a healthy subject. (a) the average value of each perfusion image as function of time. (b) - (d) perfusion images at times B, C and D in Fig. (a) and (e) the DC image at times B in Fig. (a) (Media 3).

3.1.2. Offline recording

Offline recording was chosen for the third example : following fast changing perfusion levels (e.g., the heart beat) in the dorsal side of the hand of the subject (female, 23 yr) in rest. Due to the available memory of 2 Gb in the CMOS camera we measured only for 3.8 seconds with an image size of 128×128 pixels. The recording is shown in Fig. 8. In Fig. 8(a) the average value of each perfusion image is shown as a function of time. Fig. 8(b) - (d) show the perfusion images at positions B, C and D, respectively, in Fig. 8(a) and Fig. 8(e) show the DC image at position B in Fig. 8(a).
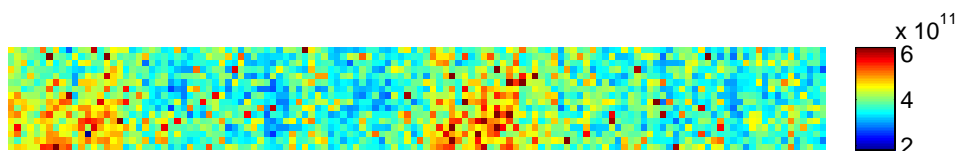
To increase length of the recorded sequence, the image size was reduced to 128×16 pixels
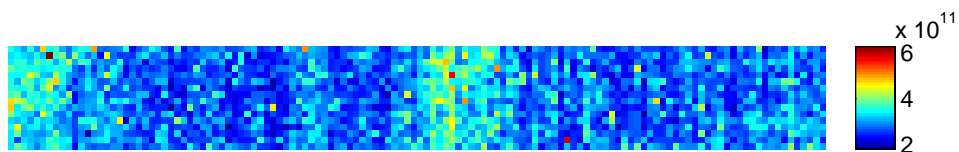
Fig. 9: Continuous recording of 128×16 pixel perfusion images in the wrist of a healthy subject. (a) the average value of each perfusion image as function of time. (b) and (c) perfusion images at times B and C in Fig. (a) ([Media 4](#)).

whereas the data were stored as 12-bits (i.e., requiring twice the amount of memory compared to 10 bits), resulting in an increase of the length of the recorded sequence in offline mode to 15.5 seconds. An occlusion was applied by inflating a blood pressure cuff around the upper arm of a healthy subject (male, 27 yr). The measurement on the wrist was started 3 minutes after the occlusion was applied. Approximately 3 seconds after the start of the measurement the occlusion was released. These results are shown in Fig. 9. In Fig. 9(a) the average value of each perfusion image is shown as a function of time, and Fig. 9(b) and (c) show the perfusion images at positions B and C, respectively, in Fig. 9(a). A clear increase in perfusion is visible after release of the occlusion.

4. Discussion

In this study, various instrumental aspects of the TOPCam have been described and the capabilities for fast imaging of skin perfusion are demonstrated. To correct for the noise in the CMOS camera, noise correction curves were measured, which for each pixel relate the noise generated contribution of the first order moment to the DC-level of that pixel. These curves were fitted with a 3rd order polynomial and the coefficients were stored. However, this fitting can induce a

small error in the calculation of the noise level. This can be seen in Fig. 4 where for some DC-values a clear difference between the raw noise curve and the fitted noise correction curve is visible. Figure 4 also shows noise measurements for the same pixel on two different days. The difference between these two measurements, which could be a temperature effect in the camera, gives an indication of the reproducibility of the noise correction curves. For low DC-levels a nice agreement is present between the measurements on the different days. For higher DC-levels a difference is visible between the two days. So the amount of noise differs significantly from one day to another. This day-by-day difference also induces a non-perfect estimation of the noise level, which results in an under- or overestimation of the perfusion level. Figure 5(b) shows the consequences of these differences between days and inaccurate noise estimation as a result of the fitting. In the ideal case the Delrin and background should both give a zero perfusion level. Due to the non-perfect pixel-by-pixel noise correction a difference is visible between the perfusion level of the Delrin and the background. The level of noise is only dependent on the properties of the camera and the detected DC level of the light, so the noise level obtained empirically on Delrin can also be used for in-vivo measurements. In Fig. 5(a) vertical stripes are present, these stripes are suppressed in Fig. 5(b) due to the applied noise correction. For low DC-values (e.g below 128 digital levels) the 3rd order deviates from the measured curves. A 4th or higher order polynomial fit removed this deviation but resulted in a deviation for higher DC-values, which is undesirable because the measurements are usually performed in that range of DC values.

The TOPCam allows us to follow the increase of perfusion in an extended tissue area, e.g., in response to the application of capsicum cream (Fig. 6). In all the images a spot with higher perfusion than the surrounding tissue is visible. This is caused by a small wound which was present at the hand of the subject during the measurement. Furthermore, TOPCam imaging revealed that the capsicum cream does not only increase the perfusion at the location where the cream was applied, but also slightly in the area around it.

In the comparison between the TOPCam and the fiberoptic laser Doppler probe (Fig. 7), a difference can be observed between the signals measured by the TOPCam and the probe, which might be caused by the different regions probed by the fiberoptic probe and the TOP-Cam. Another difference between both devices is the algorithm used to process the signal and the different measurement depth. Due to this difference in measurement depth, both devices measure a slightly different part of the micro circulation which can explain the difference in perfusion. Another difference between the two measurements is an overshoot with a duration of a few seconds after the release of the occlusion measured with the laser Doppler probe, which is not recorded by the TOPCam. A zoom-in on the overshoot (not shown) reveals that during the overshoot the TOPCam was processing the data from the previous measurement, and therefore could not measure the overshoot. Another striking detail is the variation in the signal from the TOPCam during the occlusion. Because the signal for the TOPCam is obtained by averaging over a large number of pixels, the pixel to pixel variations in optoelectronic properties should cancel out. The exact reason for this difference is not known yet.

The average time between the peaks in the continuous measurement (i.e., Fig. 8) is 746 milliseconds, resulting in a heart beat frequency of 80 beats per minute, which is in the range of normal heart frequencies. In between the heart beats some smaller variations are visible. These variations occur at a time scale of approximately 0.1 second. When the pressure wave of blood arrives at a vascular branch in larger vessels, part of the wave hits the wall and reflects back where it interferes with the end of the pressure wave. This causes variations at the time scale of approximately 0.1 second, so called dicrotic notches. However, it is unlikely that these flow variations reach the micro circulation. These small excursions of the flux signal are probably caused by overall tissue motion due to the pressure waves in the larger arteries. In the center of

the DC image (Fig. 8(e)) an area with a slightly higher intensity due to curvature of the hand is visible. In the perfusion images this area is visible with a lower perfusion, indicating the perfusion image is over-normalized.

After the release of the occlusion in the longer continuous measurement (Fig. 9) the same variations can be observed in the flux signal. The average time between the heart beat peaks is 825 milliseconds, which corresponds with a heart beat frequency of 73 beats per minute, which is in the normal range. However, during the occlusion the average perfusion level does not approach zero. This can partially be explained by the non-perfect pixel-by-pixel noise correction as discussed above. A possible other explanation is that the blood pressure cuff was not inflated completely, so the blood supply was not fully blocked. As was the case in the comparison between between the TOPCam and the laser Doppler probe from Perimed (Fig. 7), in this figure a steady decrease is visible after the first increase of perfusion after release of the occlusion. After 11 seconds the perfusion already dropped to 70% of the difference between the baseline and the first increase.

Table 2 shows that the most time consuming part in the imaging process of the TOPCam is the transfer of data from the camera to the computer to process the data. This long time is mainly caused by the protocol used by the camera to communicate with the computer. Improving this protocol will result in a considerable increase of imaging speed for uninterrupted perfusion imaging. Furthermore processing could be improved by making use of parallel processing (e.g., graphics card or dual/quatro core processor) resulting in a further increase of imaging speed.

One of the major benefits of a high speed camera based on CMOS image array technology to image perfusion is the fast imaging speed, which is superior to that of scanning beam laser Doppler perfusion imagers. Furthermore it gives the opportunity to make a photo with the same sensor that was used for the measurement. In this way the perfusion image can simply be overlayed with the photo for easy orientation. However, using a high speed CMOS camera also has some drawbacks. Due to the different amplifiers for different pixel columns, fixed pattern noise will be induced in the measurements, resulting in images which are noisier than those produced by scanning beam laser Doppler perfusion imagers. However, this issue will probably be solved by further technological sophistication. In newer CMOS-cameras, already a smaller fixed pattern noise is observed. Furthermore, analog filtering of the photocurrent fluctuations is not possible with commercial CMOS imaging arrays, so high pass filtering (i.e., to suppress moving artifacts) and low pass filtering (i.e., to prevent aliasing) can not be done. To be able to perform analog filtering custom made CMOS imaging arrays are required [28]. Due to the high imaging speed, motion artifacts will play a minor role and by selecting a high frame rate, the possibility of aliasing can be reduced. We have shown that current high speed CMOS cameras enable real time perfusion imaging, but with a lower signal-to-noise ratio than a scanning beam imager. However, since the high speed feature allows for multiple imaging and averaging, this difference in signal-to-noise ratio might partly be overcome.

5. Conclusion

In conclusion, we have presented the Twente Optical Perfusion Camera (TOPCam), a novel laser Doppler Perfusion Imager based on CMOS image array technology. To correct for the noise in the CMOS camera, noise correction curves based on a 3rd order fit through the measured noise were determined. This non-perfect fit results in an under- or overestimation of the perfusion level.

The TOPCam can be used in two different imaging modes. In the online mode data for one perfusion frame are recorded and immediately analyzed before the next measurement is performed. Using this imaging mode we can achieve a frame rate of 0.2 fps without time limitation. In the offline mode the analysis is postponed, first the data for all measurements are recorded

before the data are analyzed. Using this imaging mode we can achieve a frame rate of 26 fps for 3.87 seconds (i.e perfusion images of 128×128 pixels) up to 15.47 seconds (i.e perfusion images of 128×32 pixels) or even longer if the data are stored as 10-bit instead of 12 bit data. Using a lens with a focal length of 12 mm, we can image an area of approximately 7×7 centimeter at 40 cm distance (i.e., the normal working distance) on 128×128 pixels.

The imaging speed of the TOPCam is superior to scanning beam laser Doppler perfusion imagers. Further research is needed to characterize the imaging quality and imaging properties (e.g., measurement depth, resolution, response to different tissue types) of the TOPCam with respect to scanning beam laser Doppler perfusion imagers.

Acknowledgments